Am J Physiol Heart Circ Physiol
279: H3101–H3112, 2000.

special communication

Cellular and functional defects in a mouse model of heart failure

GIOVANNI ESPOSITO*,[1] L. F. SANTANA*,[2,3,4] KEITH DILLY*,[3] JADER DOS SANTOS CRUZ,[3,5] LAN MAO,[1] W. J. LEDERER,[2,3] AND HOWARD A. ROCKMAN[1]

[1]*Department of Medicine, Duke University Medical Center, Durham, North Carolina 27710;* [2]*Medical Biotechnology Center, University of Maryland Biotechnology Institute, and* [3]*Department of Physiology, University of Maryland School of Medicine, Baltimore, Maryland 21201;* [4]*Institute of Neurobiology, University of Puerto Rico, San Juan, Puerto Rico 00901; and* [5]*Departamento de Bioquimica e Imunologia, Laboratorio de Membranas Excitaveis, Universidade Federal de Minas Gerais, Minas Gerais, Brazil*

Received 14 January 2000; accepted in final form 26 June 2000

Esposito, Giovanni, L. F. Santana, Keith Dilly, Jader Dos Santos Cruz, Lan Mao, W. J. Lederer, and Howard A. Rockman. Cellular and functional defects in a mouse model of heart failure. *Am J Physiol Heart Circ Physiol* 279: H3101–H3112, 2000.—Heart failure and dilated cardiomyopathy develop in mice that lack the muscle LIM protein (MLP) gene ($MLP^{-/-}$). The character and extent of the heart failure that occurs in $MLP^{-/-}$ mice were investigated using echocardiography and in vivo pressure-volume (P-V) loop measurements. P-V loop data were obtained with a new method for mice (sonomicrometry) using two pairs of orthogonal piezoelectric crystals implanted in the endocardial wall. Sonomicrometry revealed right-shifted P-V loops in $MLP^{-/-}$ mice, depressed systolic contractility, and additional evidence of heart failure. Cellular changes in $MLP^{-/-}$ mice were examined in isolated single cells using patch-clamp and confocal Ca^{2+} concentration ($[Ca^{2+}]$) imaging techniques. This cellular investigation revealed unchanged Ca^{2+} currents and Ca^{2+} spark characteristics but decreased intracellular $[Ca^{2+}]$ transients and contractile responses and a defect in excitation-contraction coupling. Normal cellular and whole heart function was restored in $MLP^{-/-}$ mice that express a cardiac-targeted transgene, which blocks the function of β-adrenergic receptor (β-AR) kinase-1 (βARK1). These data suggest that, despite the persistent stimulus to develop heart failure in $MLP^{-/-}$ mice (i.e., loss of the structural protein MLP), downregulation and desensitization of the β-ARs may play a pivotal role in the pathogenesis. Furthermore, this work suggests that the inhibition of βARK1 action may prove an effective therapy for heart failure.

contractility; β-adrenergic receptor; excitation-contraction coupling; calcium signaling; transgenic; β-adrenergic receptor kinase

HEART FAILURE IS a clinical syndrome in which molecular and cellular changes in cardiac myocytes lead to inadequate myocardial function. Much attention has been focused on the role played by the β-adrenergic receptor (β-AR) signaling pathway in heart failure after the surprising discovery that β-AR blockers, known to have negative inotropic action, provide benefit to patients in heart failure (4–6). Indeed, it has been well established that β-ARs are downregulated and/or desensitized during heart failure (3). Characteristic changes in β-ARs include uncoupling of both β_1- and β_2-AR subtypes, threefold increase in activity of the β-adrenergic receptor kinase (βARK1), and increased levels of G_i (13, 40). Exploration of the mechanism of action of β-AR modulation in the context of heart failure requires cellular and molecular examination of cardiac myocytes from animals whose myocardial function is well defined.

A useful genetically defined murine model of heart failure was recently described (1). In this model, the muscle LIM protein (MLP) is knocked out to produce the $MLP^{-/-}$ animal. Two genetic interventions have been described that suggest that alterations in either Ca^{2+} transport (29, 38) or β-AR function (31) play a central role in $MLP^{-/-}$ heart failure. We investigated the nature and extent of heart failure associated with the $MLP^{-/-}$ mouse, and that rescued by the βARK1 inhibitor, by examining the intrinsic myocardial contractile state in vivo using a pressure-volume (P-V) analysis and intracellular Ca^{2+} concentration ($[Ca^{2+}]_i$) signaling using patch-clamp methods and confocal

*G. Esposito, L. F. Santana, and K. Dilly contributed equally to this work.

Address for reprint requests and other correspondence: H. A. Rockman, Dept. of Medicine, Duke Univ. Medical Center, DUMC 3104, Durham, NC 27710 (E-mail: h.rockman@duke.edu).

The costs of publication of this article were defrayed in part by the payment of page charges. The article must therefore be hereby marked "*advertisement*" in accordance with 18 U.S.C. Section 1734 solely to indicate this fact.

Ca^{2+} imaging. We present here data showing that $MLP^{-/-}$ animals have a defect in excitation-contraction (EC) coupling that contributes to their contractile dysfunction and that this pathology is significantly more severe than the loss of the MLP per se. Moreover, β-AR dysfunction appears to be a necessary component because restoration of β-AR signaling in these animals is sufficient to prevent the abnormalities of in vivo contractile dysfunction, of poor cellular contraction, of weak Ca^{2+} signaling, and of defective EC coupling.

METHODS

Experimental Animals

Adult $MLP^{-/-}$ and $MLP^{-/-}$/βARK1 inhibitor (βARKct) littermate mice of either sex, age 5 to 7 mo, were used in this study. The mice were generated by mating transgenic mice with cardiac-targeted overexpression of the βARKct (24) with mice homozygous for the deletion of the MLP gene ($MLP^{-/-}$) (1) to create $MLP^{-/-}$/βARKct mice (31). Nonlittermate wild-type mice of either 129Sv/B6 or CD-1 strain were used as controls. The animals in this study were handled according to approved protocols and animal welfare regulations of the authors' Institutional Review Boards.

Transthoracic Echocardiography

Two-dimensional (2D) guided M-mode echocardiography was performed using an HDI 5000 echocardiograph (ATL, Bothell, WA) as previously described (11, 31). Mice were first studied in the conscious state using gentle manual restraint after a period of acclimation. A soft plastic collar was fashioned to prevent the animals from biting the probe. After acquisition of satisfactory echocardiograms, the same mice were restudied under anesthesia (Avertin 2.5%, 14 μl/g ip).

P-V Loops

Several days after echocardiography, mice were reanesthetized with a mixture of ketamine (100 mg/kg) and xylazine (2.5 mg/kg) and were connected to a rodent ventilator after endotracheal intubation. After bilateral vagotomy, the chest was opened and the pericardium was dissected to expose the heart. A 7-0 suture ligature was placed around the transverse aorta to manipulate loading conditions (see Fig. 2*A*). A 1.4-Fr (0.46 mm) high-fidelity micromanometer catheter (Millar Instruments, Houston, TX) was inserted into the right carotid and advanced retrograde into the left ventricle (LV). A polyethylene (PE)-50 catheter was inserted into the external jugular vein for drug infusion. Two pairs of miniature omnidirectional piezoelectric crystals (0.7 mm; Sonometrics, London, ON, Canada) were implanted in the endocardium of the LV by inserting the crystals through the epicardial layer into the chamber and then withdrawing until there was resistance. Short-axis dimension was measured with a pair of crystals implanted in the anterior-posterior orientation. Long-axis dimension was measured with a crystal implanted in the apex and one crystal attached to the base of the heart at the level of the aortic valve using cyanoacrylate adhesive (Vetbond, 3M Animal Care Products, St. Paul, MN). The space and time resolution of the sonomicrometry system are 0.015 mm and 0.001 s, respectively.

After a brief period of stabilization, simultaneous LV pressure and LV dimensions were recorded at baseline and during increases in afterload generated by gently pulling on the suture to transiently constrict the transverse aorta. The ventilator was stopped during data acquisition to eliminate effects of positive ventilation. After return of LV pressure to baseline values, the contractile state was increased with a dobutamine infusion ($2\ \mu g \cdot kg^{-1} \cdot min^{-1}$). After steady state was reached (~5 min), recordings of variably loaded pressure-dimension measurements were made as above. All data was recorded digitally at 2,000 Hz and stored on a computer for off-line analysis. At the end of the experiment, animals were killed and proper positioning of the crystals was documented by direct inspection.

Data Analysis

The digitized data were analyzed using a computer algorithm. Baseline and dobutamine hemodynamic values were obtained by averaging 10 beats recorded during the steady-state periods. Parameters measured were LV systolic and end-diastolic pressure, maximal (LV dP/dt_{max}) and minimal first derivative of LV pressure, and heart rate. The end-systolic point of each P-V loop was determined by an automated iterative linear regression technique as previously described (21, 30). LV volume was calculated as a modified general ellipsoid using the equation $V = (\pi/6) \cdot D_{la} \cdot (D_{ap})^2$ where D_{la} is the apex to base long-axis LV dimension and D_{ap} is the anterior to posterior short-axis LV dimension. The end-systolic points were then fitted to a parabolic curvilinear model, $P_{es} = a(V_{es} - V_0)^2 + b(V_{es} - V_0)$, where P_{es} is end-systolic pressure, V_{es} is end-systolic volume, V_0 is the volume axis intercept, b is the local slope at V_0, and a is the curvilinearity coefficient (21). If the 95% confidence interval of a did not include zero, the end-systolic P-V relation (ESPVR) was considered curvilinear (see Table 3).

Cell Isolation and Electrophysiology

Adult animals (wild type, $n = 5$; $MLP^{-/-}$, $n = 6$; and $MLP^{-/-}$/βARKct, $n = 7$) were killed by intraperitoneal injection of pentobarbital sodium (100 mg/kg). Single mouse ventricular myocytes were isolated (37) and stored at room temperature (22–25°C) in Dulbecco's modified Eagle's medium (JRH Biosciences, Lanexa, KS) until being used. An Axopatch-200A amplifier (Axon Instruments) was used to patch clamp the cells (whole cell configuration) and measure membrane currents. Patch pipettes of nominal resistance of 0.5–3 MΩ were used and were filled with an internal solution of (in mM) 130 CsCl, 20 tetraethylammonium chloride, 5 Mg-ATP, 10 HEPES, and 0.05 fluo 3-K_5; pH 7.2 (with NaOH). Some cells were preloaded with fluo 3 by 30-min exposure to 1.5 μM fluo 3-AM at room temperature.

Cells were superfused with one of three solutions. *Solution 1* contained (in mM) 140 NaCl, 5 KCl, 0.5 $MgCl_2$, 1.8 $CaCl_2$, 0.33 NaH_2PO_4, 5.5 glucose, and 5 HEPES. *Solution 2* contained (in mM) 140 NaCl, 5 CsCl, 0.5 $MgCl_2$, 1.8 $CaCl_2$, 0.33 NaH_2PO_4, 5.5 glucose, and 5 HEPES. *Solution 2* was used to measure Ca^{2+} current (I_{Ca}). *Solution 3* contained (in mM) 145 CsCl, 0.5 $MgCl_2$, 5.5 glucose, and 5 HEPES. This solution was used to block the Na^+/Ca^{2+} exchanger when the sarcoplasmic reticulum (SR) Ca^{2+} content was tested by applying 20 mM caffeine. The pH of all extracellular solutions was kept at 7.4 with the temperature at 34–37°C.

Confocal Microscopy and $[Ca^{2+}]_i$ Measurements

Confocal microscopy was used to measure $[Ca^{2+}]_i$ (7–9) and to investigate cellular function as previously described in rat and mouse heart cells (16, 36, 37). A robust preloading protocol was used to attain similar SR Ca^{2+} loads (35, 37).

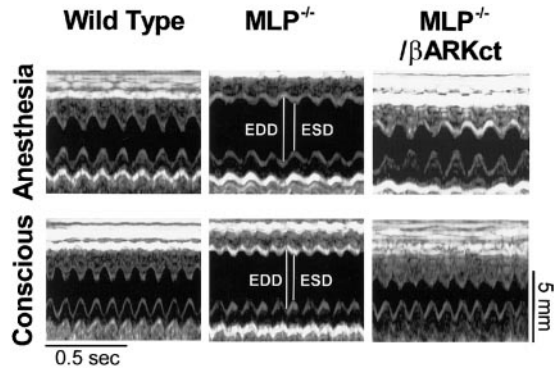

Fig. 1. Echocardiography in conscious and anesthetized wild-type, muscle LIM protein (MLP) knockout ($MLP^{-/-}$), and $MLP^{-/-}$/β-adrenergic receptor kinase-1 inhibitor (βARKct) mice. Representative M-mode echocardiographic tracings are shown for the same mouse under anesthesia and in the conscious state. The white lines indicate left ventricular (LV) end-diastolic dimension (EDD) and end-systolic dimension (ESD). Although the $MLP^{-/-}$ mouse shows an enlarged chamber with reduced cardiac performance under both conscious and anesthetized conditions, chamber diameter and cardiac performance are normal in the $MLP^{-/-}$/βARKct mouse.

We were therefore able to compare Ca^{2+} signaling in cells from wild-type, $MLP^{-/-}$, and $MLP^{-/-}$/βARKct animals because they had a constant amount of Ca^{2+} in the SR (15). This procedure permits meaningful comparison of EC coupling gain (35, 37).

Statistical Analysis

Data are expressed as means ± SE. Two-way repeated ANOVA was used to evaluate the hemodynamic measurements, the ESPVR variables under basal conditions and with dobutamine stimulation, and the echocardiographic parameters between anesthetized and conscious states. When appropriate, post hoc analysis was performed with a Newman-Keuls test. Bland-Altman (2) analysis (coefficient of variability) was used to show agreement between the crystal and echocardiographic measurements of LV diastolic dimension. For all analyses, $P < 0.05$ was considered significant. For the data from single-cell experiments, two-sample comparisons were performed using Student's *t*-test, and multigroup comparisons were made using a one-way ANOVA and Tukey's test.

RESULTS

Heart Failure in $MLP^{-/-}$ Mice

Evidence from echocardiographic studies. Investigations into the nature and extent of heart failure associated with the $MLP^{-/-}$ mouse are shown in Fig. 1. Echocardiograms performed in mice under both conscious and anesthetized conditions for wild-type (Fig. 1, *left*), $MLP^{-/-}$ (Fig. 1, *middle*), and a genetically crossed hybrid mouse (Fig. 1, *right*) are shown. From Fig. 1, it is clear that the $MLP^{-/-}$ mice have hearts with significantly enlarged internal chamber dimensions [end-diastolic dimension (EDD) and end-systolic dimension (ESD)] and reduced fractional shortening compared with wild-type mice (see Fig. 1 and Table 1). Such LV dilation and reduced cardiac function are apparent in both anesthetized and conscious animals. Although echocardiography is valuable to measure chamber size and systolic performance in heart failure in vivo, it is limited in the assessment of the intrinsic contractile state of the ventricle because of the dependence on afterload (26). To examine the murine myocardial contractile state in vivo, a new method was developed for use in mice: sonomicrometry pressure-volume analysis (See Fig. 2*A*).

Cardiac function assessed using P-V loop measurements. With two pairs of endocardial implanted piezoelectric crystals (see METHODS and Fig. 2*A*) and a high-fidelity micromanometer in the LV, in vivo P-V relationships were obtained. These P-V relationships were obtained at different "loading" conditions and in the presence and absence of β-AR stimulation. P-V relationships provide a powerful approach to examine contractile function in vivo (20, 33), and these measurements were used to investigate in vivo contractile dysfunction in the $MLP^{-/-}$ mice.

Representative P-V loop families are shown for a typical wild-type mouse in Fig. 2*B*. At baseline the end-diastolic volume (V_{ed}) is 32 μl, which increases to 55 μl as afterload is increased by aortic constriction, as shown by the shift to the right and upwards as expected for a normal heart (Fig. 2*B* and Table 2). The addition of the β-AR agonist dobutamine (2 $\mu g \cdot kg^{-1} \cdot$

Table 1. *Echocardiographic parameters in conscious and anesthetized gene-targeted mice*

	Wild Type (n = 10)		$MLP^{-/-}$ (n = 10)		$MLP^{-/-}$/βARKct	
	Anesthesia	Conscious	Anesthesia	Conscious	Anesthesia	Conscious
LVEDD, mm	3.6 ± 0.04	3.4 ± 0.05[a]	4.7 ± 0.19[d]	4.7 ± 0.20[d]	3.7 ± 0.13[f]	3.5 ± 0.10[af]
LVESD, mm	1.9 ± 0.09	1.5 ± 0.07[a]	3.5 ± 0.22[d]	3.4 ± 0.24[d]	1.7 ± 0.14[f]	1.4 ± 0.12[af]
FS, %	47 ± 2.8	55 ± 2.4[b]	26 ± 2.0[d]	29 ± 2.8[d]	53 ± 3.1[cf]	59 ± 2.6[af]
T_{SEP}, mm	0.7 ± 0.03	0.8 ± 0.03	0.7 ± 0.05	0.7 ± 0.07	0.9 ± 0.05[cf]	1.0 ± 0.05[cf]
T_{PW}, mm	0.6 ± 0.03	0.6 ± 0.02	0.6 ± 0.03	0.7 ± 0.05	0.8 ± 0.07[ce]	0.8 ± 0.07[ce]
HR, beats/min	539 ± 21	660 ± 19[b]	490 ± 46	622 ± 18[b]	453 ± 54	632 ± 24[b]
mean V_{cfc}, circ/s	3.49 ± 0.23	4.38 ± 0.24	2.02 ± 0.19[d]	2.74 ± 0.57[d]	4.28 ± 0.29[cf]	5.44 ± 0.39[acf]

Values are means ± SE; n, no. of mice. $MLP^{-/-}$, muscle LIM protein knockout mice; βARKct, β-adrenergic receptor kinase inhibitor; LV, left ventricle; LVEDD, LV end-diastolic dimension; LVESD, LV end-diastolic dimension; FS, fractional shortening; T_{SEP}, septal wall thickness; T_{PW}, posterior wall thickness; HR, heart rate; V_{cfc}, HR-corrected velocity of circumferential fiber shortening. [a]$P < 0.05$, [b]$P < 0.001$ vs. anesthesia of same genotype; [c]$P < 0.05$, [d]$P < 0.001$ vs. wild-type anesthesia or wild-type conscious; [e]$P < 0.05$, [f]$P < 0.001$ vs. $MLP^{-/-}$ anesthesia or $MLP^{-/-}$ conscious.

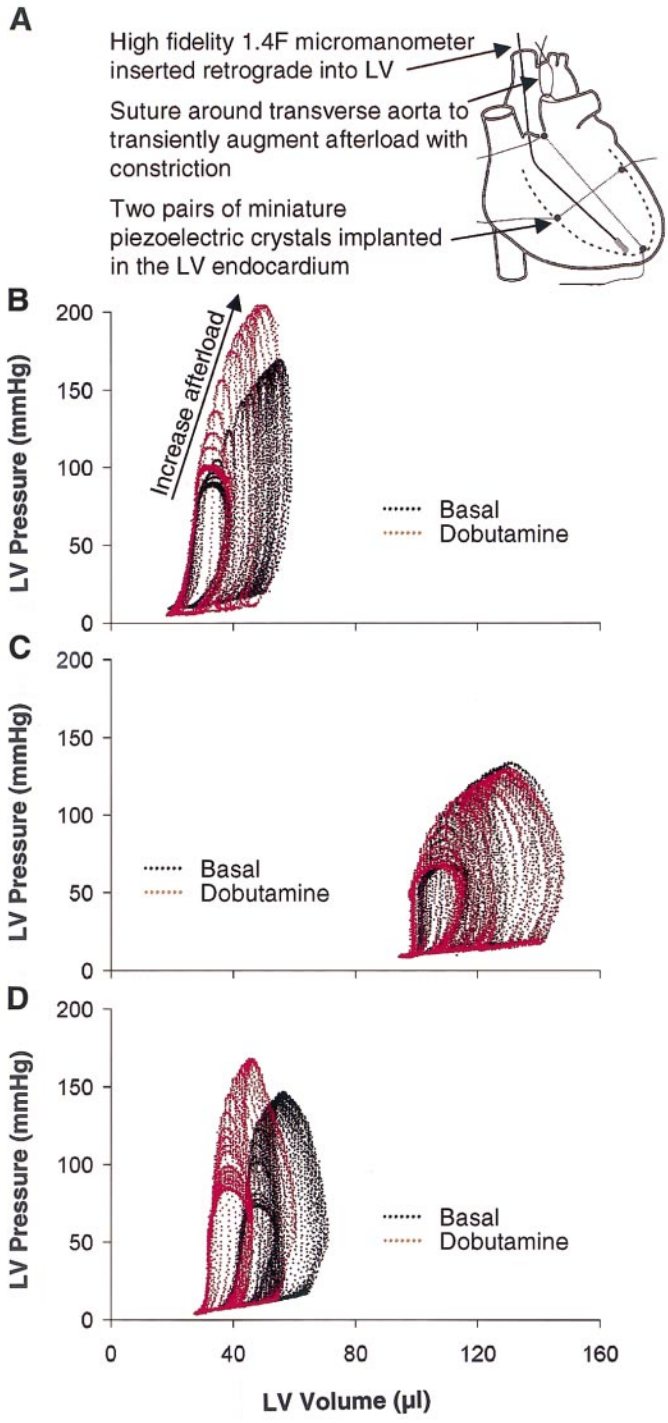

Fig. 2. Pressure-volume (P-V) loops in wild-type, $MLP^{-/-}$, and $MLP^{-/-}$/βARKct mice. *A*: schematic of the instrumented mouse heart. Representative P-V loops are displayed during transient constriction of the transverse aorta to augment afterload under basal conditions (black) and after dobutamine ($2\ \mu g \cdot kg^{-1} \cdot min^{-1}$) infusion (red) for wild-type heart (*B*), $MLP^{-/-}$ heart (*C*), and $MLP^{-/-}$/βARKct heart (*D*).

min^{-1}, red P-V loops) slightly increases the LV end-systolic pressure (LVESP) with low afterload but has an even more dramatic action as afterload is increased. More importantly, however, there is an increase in the slope of the relation describing end-systolic pressure and volume as afterload increases (Figs. 2*B* and 3*A*). This pattern of changes in cardiac function is typical for a normal heart whether it be from a mouse, dog, pig, or human (19, 20, 22, 33) and is a fingerprint for the normal myocardial response to increased afterload in the presence and absence of β-AR stimulation.

The P-V relationships observed in animals lacking the muscle LIM protein ($MLP^{-/-}$) are dramatically different from those observed in wild-type mice. The V_{es} and V_{ed} of the hearts are dramatically increased (7-fold and 4-fold, respectively), and fractional shortening is significantly reduced from 47–55% in control animals to 26–29% in $MLP^{-/-}$ animals ($P < 0.001$). The responses to increases in afterload are less steep in $MLP^{-/-}$ animals (Fig. 3*A*, Table 3) compared with wild-type hearts, and there is little change in the slope of the ESPVR in response to the β-AR agonist dobutamine (Figs. 2*C* and 3*A*). Together, these data indicate that $MLP^{-/-}$ mice are in functional heart failure, a finding consistent with clinical observation of these animals. These data also support the large body of published work indicating that the β-AR signaling system is poorly responsive or unresponsive in many models of heart failure (3). It is also worth noting that although LV dP/dt_{max} is mildly reduced in the $MLP^{-/-}$ mice compared with wild-type mice, it does not have the sensitivity to detect the marked abnormalities in intrinsic contractility as shown by the P-V loop analysis (12, 27).

To test whether this measure of cardiac function (P-V analysis) in mice agrees with an established standard (echocardiography), we compared cardiac dimensions determined by sonomicrometry and by echocardiography in the same mice. Figure 4*A* shows that the LVEDD measured by the two methods was similar, with the sonomicrometry giving only a slightly larger dimension. Furthermore, a Bland-Altman analysis (Fig. 4*B*) showed a good agreement between the two in vivo measurements of LV diastolic dimension.

EC Coupling Defect in $MLP^{-/-}$ Mice

Cellular function. The cellular cause of the contractile dysfunction in $MLP^{-/-}$ mice is unknown. However, Arber et al. (1) suggested that the absence of the MLP, a structural protein in striated muscle, might be responsible. Although this hypothesis seems reasonable, Ca^{2+} signaling defects in heart failure have been detected in other models of heart failure even when alternative reasonable causes were found (16, 41). Consequently, we decided to test the possibility that Ca^{2+} signaling may be altered and may contribute to the heart failure phenotype in $MLP^{-/-}$ mice. We examined membrane currents, $[Ca^{2+}]_i$, and cellular shortening and relaxation in patch-clamped heart cells (whole cell mode). Figure 5*A* shows the voltage protocol, the $[Ca^{2+}]_i$ measurement as fractional fluorescence (F/F_o), the shortening record, and the membrane current density (pA/pF) in a single control heart cell. It is clear from the data that the cardiomyocytes from $MLP^{-/-}$

Table 2. *Steady-state hemodynamic variables in open-chest instrumented mice*

	Wild Type (n = 8)		MLP$^{-/-}$ (n = 8)		MLP$^{-/-}$/βARKct (n = 8)	
	Basal	Dobutamine	Basal	Dobutamine	Basal	Dobutamine
LVSP, mmHg	79.6 ± 5.3	89.6 ± 6.8[a]	63.9 ± 4.9	74.6 ± 8.4	65.7 ± 4.0	79.7 ± 3.8[a]
LVEDP, mmHg	4.6 ± 0.4	2.9 ± 0.7	4.4 ± 0.5	5.8 ± 0.7[c]	4.5 ± 0.7	2.9 ± 0.6[e]
LV dP/dt_{max}, mmHg/s	3,939 ± 230	6,459 ± 635[b]	3,633 ± 354	4,413 ± 329[d]	4,383 ± 297	7,085 ± 716[bf]
V_{es}, μl	31 ± 3.0	27 ± 2.0	112 ± 17	105 ± 16[a]	42 ± 4[cf]	38 ± 4[cf]
V_{ed}, μl	43 ± 4.0	39 ± 3.0	125 ± 18[d]	118 ± 17[ad]	55 ± 6[cf]	52 ± 6[df]
HR, beats/min	355 ± 25	449 ± 23[b]	315 ± 16	399 ± 22[b]	334 ± 22	417 ± 21[b]
BW, g	36.2 ± 1.7		34.4 ± 0.5		38.9 ± 3.2	

Values are means ± SE; n = no. of mice. LVSP, LV systolic pressure; LVEDP, LV end-diastolic pressure; dP/dt_{max}, maximal first derivative of pressure; V_{es}, end-systolic volume; V_{ed}, end-diastolic volume; BW, body wt. [a]$P < 0.05$, [b]$P < 0.001$ vs. basal of same genotype; [c]$P < 0.05$, [d]$P < 0.001$ vs. wild-type basal or wild-type dobutamine; [e]$P < 0.05$, [f]$P < 0.001$ vs. MLP$^{-/-}$ basal or MLP$^{-/-}$ dobutamine.

mice produce significantly smaller $[Ca^{2+}]_i$ changes and reduced contractions for similar Ca^{2+} currents (see Fig. 5*B*). These differences are demonstrated more clearly when the voltage dependence for these data is shown in Fig. 6. There is also a clear reduction in the rate of cellular shortening shown in Fig. 5. Figure 6*D* shows the voltage dependence decrease in shortening and relaxation in the cardiac myocytes taken from MLP$^{-/-}$ animals.

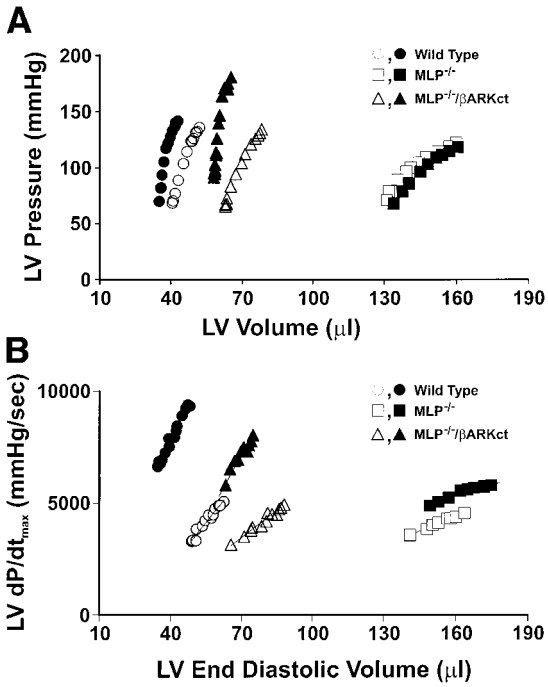

Fig. 3. LV end-systolic P-V relation (ESPVR) and LV maximal first derivative of pressure (dP/dt_{max})-end diastolic volume (V_{ed}) relations. *A*: representative LV ESPVR are plotted for wild-type, MLP$^{-/-}$, and MLP$^{-/-}$/βARKct mice under basal conditions (open symbols) and with dobutamine infusion (closed symbols). The P-V relations were fit by multiple linear regression to a second-order polynomial and solved for the regression coefficients a, b, and V_0 (see Table 3). *B*: representative LV dP/dt_{max}-V_{ed} relationships for animals as noted in *A*. The LV dP/dt_{max}-V_{ed} relationship is a sensitive load-independent measure of contractile performance (30). The slope of the LV dP/dt_{max}-V_{ed} relation is significantly greater in wild-type (87.4 ± 25.1 mmHg·s^{-1}·μl^{-1}; n = 5) than in MLP$^{-/-}$ (41.3 ± 7.0, mmHg·s^{-1}·μl^{-1}; n = 6, $P < 0.01$) mice but not different from MLP$^{-/-}$/βARKct mice (82.2 ± 16.7 mmHg·s^{-1}·μl^{-1}, n = 6). Dobutamine (filled symbols) markedly increases the slope of the dP/dt_{max}-V_{ed} relationship in wild-type and MLP$^{-/-}$/βARKct animals but elicits little response in MLP$^{-/-}$ mice.

To better understand the reduced contractility found in vivo using a P-V analysis, we examined the dependence of cellular shortening on $[Ca^{2+}]_i$ during the contractile cycle at representative depolarizations (−20, 0, and +20 mV), as shown in Fig. 7. There is a clear hysteresis in the relationship, as illustrated in Fig. 7*A*, *middle*. The arrows along the dashed line reveal the trajectory of the plot. The hysteresis reflects the rapid release of Ca^{2+} by the EC coupling mechanism (Ca^{2+}-induced Ca^{2+} release, CICR) and the relatively slower responsiveness of the contractile machinery. Hysteresis in wild-type mouse heart cells is expected because of the known kinetics of contraction. In MLP$^{-/-}$ animals, the heart cells show a characteristic flattened hysteresis loop. This can be seen best if one compares Fig. 7*A*, *left*, with Fig. 7*B*, *middle*. These examples have a similar elevation of $[Ca^{2+}]_i$, but the extent of the shortening is considerably decreased (~5%) in the MLP$^{-/-}$ animals compared with controls (~10%). The data in Fig. 7*B* show the consistent pattern of reduced contractile responsiveness to $[Ca^{2+}]_i$ changes. The reduced extent of contraction leads to the flattened appearance of each of the trajectories shown in Fig. 7*B*. Together, the data suggest that, in addition to the decreased shortening due to the reduction in the $[Ca^{2+}]_i$ transients (as shown in Fig. 6*C*), there is a further reduction in contractility due to an additional factor that has not yet been defined. In MLP$^{-/-}$ heart failure, the additional factor may be alterations in troponin or other contractile proteins that have been observed in heart failure (28, 39) or may be directly related to the chronic loss of MLP.

The contractile defects revealed in Figs. 5, 6, and 7 are further examined in Fig. 8*A*, where peak shortening is plotted against peak $[Ca^{2+}]_i$. There is the clear trend that the steep relationship seen in cells from wild-type animals is less steep in cells from the MLP$^{-/-}$ animals. This reinforces the data shown in Fig. 7 but does not answer the question of considerable interest. Why is the $[Ca^{2+}]_i$ transient reduced in the cells from the MLP$^{-/-}$ mice?

To determine why the $[Ca^{2+}]_i$ transients are smaller in MLP$^{-/-}$ mice, experiments were done under conditions that produce similar SR loading (16, 35, 37, 41).

Table 3. *End-systolic pressure-volume relations in gene-targeted mice*

	Wild Type (n = 8)		MLP$^{-/-}$ (n = 8)		MLP$^{-/-}$/βARKct (n = 8)	
	Basal	Dobutamine	Basal	Dobutamine	Basal	Dobutamine
a, mmHg/μl^2	−0.521 ± 0.191	−0.941 ± 0.235[a]	−0.110 ± 0.034[c]	−0.110 ± 0.041[d]	−0.610 ± 0.152[e]	−1.336 ± 0.280[bcf]
b, mmHg/μl	14.9 ± 2.7	22.6 ± 3.2[b]	7.1 ± 1.1[d]	7.9 ± 1.1[d]	17.9 ± 2.6[f]	28.1 ± 3.6[bcf]
V_0, μl	27 ± 3.0	27 ± 2.0	98 ± 13[d]	94 ± 14[d]	40 ± 4.0[df]	37 ± 4.0[df]
r^2	0.990 ± 0.024	0.989 ± 0.020	0.989 ± 0.012	0.978 ± 0.010	0.994 ± 0.024	0.982 ± 0.010

Values are means ± SE; n, no. of mice. The slope of the end-systolic pressure-volume relation (ESPVR) at volume axis intercept (V_0) (coefficient b) is a measure of the intrinsic contractile state of the ventricle (23, 30). The b coefficient in MLP$^{-/-}$ mice was significantly reduced compared with both wild-type and MLP$^{-/-}$/βARKct mice, indicating decreased contractility. In contrast, the mean value for b at baseline was not statistically different between wild-type and MLP$^{-/-}$/βARKct mice, indicating rescue of contractile function by the βARKct in MLP$^{-/-}$ mice. In response to dobutamine infusion, b (slope of ESPVR) increased significantly in the wild-type and the MLP$^{-/-}$/βARKct mice, indicating augmentation to a higher contractile state. Little change in b was found in the MLP$^{-/-}$ mice with infusion of dobutamine, indicating that contractility of the MLP$^{-/-}$ ventricle was unresponsive to β-AR stimulation. The coefficient a indicates the extent of deviation from linearity (index of curvilinearity). Coefficient a was significantly different in the MLP$^{-/-}$ mice compared with both wild-type and MLP$^{-/-}$/βARKct mice. With dobutamine, a did not change in MLP$^{-/-}$ mice but significantly increased in the wild-type and MLP$^{-/-}$/βARKct animals, indicating increased curvilinearity of the ESPVR. Finally, the V_0 of the curvilinearity relation was significantly greater in the MLP$^{-/-}$ animals, indicating increased chamber volumes compared with both wild-type and MLP$^{-/-}$/βARKct mice. For all coefficients (a, b, V_0), no difference was observed between wild-type and MLP$^{-/-}$/βARKct mice. [a]$P < 0.05$, [b]$P < 0.001$ vs. basal of same genotype; [c]$P < 0.05$, [d]$P < 0.001$ vs. wild-type basal or wild-type dobutamine; [e]$P < 0.05$, [f]$P < 0.001$ vs. MLP$^{-/-}$ basal or MLP$^{-/-}$ dobutamine.

This control is important because changes in SR Ca^{2+} load alone can account for changes in EC coupling gain (35, 37). Under such conditions, there are at least two clear ways by which the $[Ca^{2+}]_i$ transient can be reduced. First, the elementary units of SR Ca^{2+} release, the Ca^{2+} sparks, can be altered. They could be smaller or shorter in duration, for example. Figure 8*B* shows typical Ca^{2+} sparks from cells taken from control and MLP$^{-/-}$ animals. The Ca^{2+} sparks are found to be indistinguishable, as shown in the sample records and the signal-averaged Ca^{2+} sparks. Second, EC coupling gain could be altered (16, 34, 37, 41). The EC coupling gain function indicates how well I_{Ca} activates SR Ca^{2+} release. At negative potentials (i.e., negative to −20 mV), the single-channel current is largest, and the opening of a single L-type Ca^{2+} channel can activate an elementary SR Ca^{2+}-release unit (9), a Ca^{2+} spark (9, 34). Thus it is at these negative potentials where EC coupling gain reflects the efficacy of the coupling between Ca^{2+} influx through L-type Ca^{2+} channels and the triggered response known as CICR (9, 34). Thus we note at negative potentials in Fig. 8*C* that there is a significant reduction in EC coupling gain in MLP$^{-/-}$ myocytes compared with control myocytes. At more positive potentials (0 and +20 mV), the single-channel current of L-type Ca^{2+} channels is reduced, and the opening of a single L-type Ca^{2+} channel is not sufficient to activate a Ca^{2+} spark. Thus, as test depolarizations reach more positive potentials, local $[Ca^{2+}]_i$ becomes relatively less important and global (i.e., cell wide) $[Ca^{2+}]_i$ becomes more important. For that reason, EC coupling gain declines and differences in EC coupling gain between wild-type and MLP$^{-/-}$ cells vanish (see Ref. 34). It is important to remember that in this analysis, SR Ca^{2+} load is being artificially kept constant to permit comparison of EC coupling gain in cells from the different mouse types. The reduction of EC coupling gain in MLP$^{-/-}$ heart cells indicates that the efficacy of activation of Ca^{2+} sparks by Ca^{2+} influx through the L-type Ca^{2+} channel is reduced in MLP$^{-/-}$

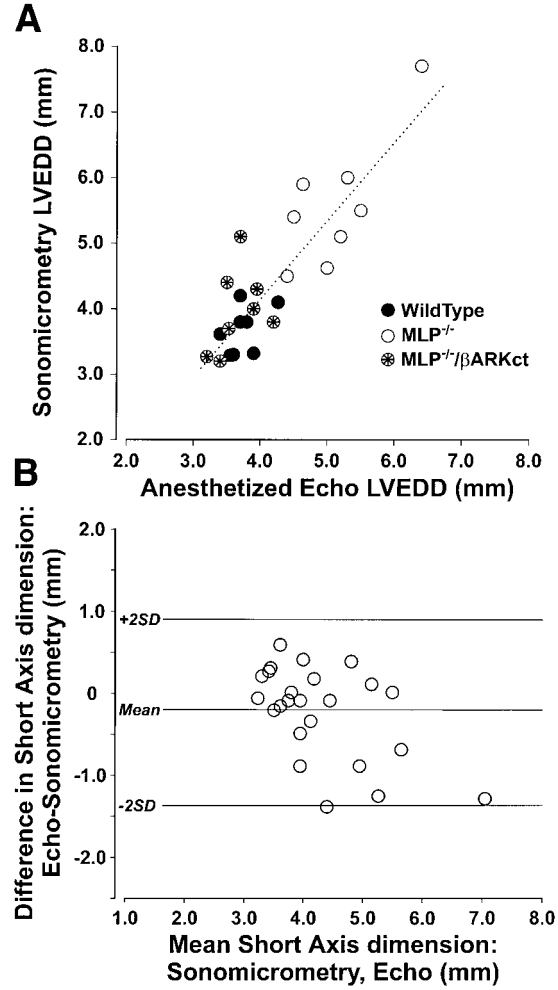

Fig. 4. Sonomicrometry vs. echocardiography. *A*: the relationship of LVEDD obtained by echocardiography to that measured by piezoelectric crystals in the short axis is shown for the 3 groups of mice. The 2 measurements correlate well, and both indicate that the diastolic dimension in the MLP$^{-/-}$ mice is much larger than that in wild-type or MLP$^{-/-}$/βARKct animals. *B*: Bland-Altman analysis showing good agreement between the 2 measurements of EDD using the 2 different techniques.

heart cells (16). This important observation provides us with the primary evidence that there is a defect in EC coupling in MLP$^{-/-}$ myocardial cells.

βARKct Transgene Expressed in MLP$^{-/-}$ Mice

In vivo function. We examined the effect of overexpression of the βARKct transgene on cardiac function. The expression of this transgene largely prevents the downregulation and desensitization of the β-AR by inhibiting the action of βARK1 to phosphorylate the receptor (31). Figure 1, *right*, shows that cardiac function measured by echocardiography has largely returned to normal, a finding similar in principle to our earlier report (31) but now refined by improved anesthesia and echocardiography techniques. Most importantly, however, the P-V analysis shown in Fig. 2*D* is remarkable. It shows that the most dramatic change in the MLP$^{-/-}$/βARKct animals is the reduction in end-diastolic and end-systolic cardiac volumes, which have become near normal. Just as important is the increased steepness of the ESPVR with increasing afterload, which approaches that observed in wild-type animals. Furthermore, the increased slope in the ESPVR after the application of the β-AR agonist dobutamine seen in wild-type animals is restored in the MLP$^{-/-}$/βARKct animals. This functional restoration of heart function in the MLP$^{-/-}$/βARKct animals is also clearly shown in Fig. 3. These data are also supported by the LV/body weight data showing normalization of cardiac mass in the MLP$^{-/-}$/βARKct mice (wild type 3.28 ± 0.03 mg/g, MLP$^{-/-}$ 5.13 ± 0.21 mg/g, MLP$^{-/-}$/βARKct 3.55 ± 0.33 mg/g; $P < 0.005$ MLP$^{-/-}$ vs. either wild type or MLP$^{-/-}$/βARKct).

Cellular function in cells from MLP$^{-/-}$/βARKct animals. The decrease in $[Ca^{2+}]_i$ transient observed in cells from the hearts of the MLP$^{-/-}$ mice is profound. There is, however, a remarkable change in the $[Ca^{2+}]_i$ transients of the heart cells in the MLP$^{-/-}$/βARKct animals, as shown in Fig. 5*C*. Similarly, the cellular contractions are restored to the control levels as are rates of shortening and relaxation. These alterations in $[Ca^{2+}]_i$ and cell shortening are observed widely over the voltage range −40 to +50 mV, as shown in Fig. 6, B and *C*. Importantly, the Ca^{2+} current density (pA/pF) is identical for cells from control, MLP$^{-/-}$, and MLP$^{-/-}$/βARKct animals. The dependence of cell shortening as a function of $[Ca^{2+}]_i$ for the cells from MLP$^{-/-}$/βARKct animals, as shown in Fig. 7*C*, is very close to that of the wild-type animals. Compare, for example, the similarity of the shape in the sample records from wild-type and MLP$^{-/-}$/βARKct cells at

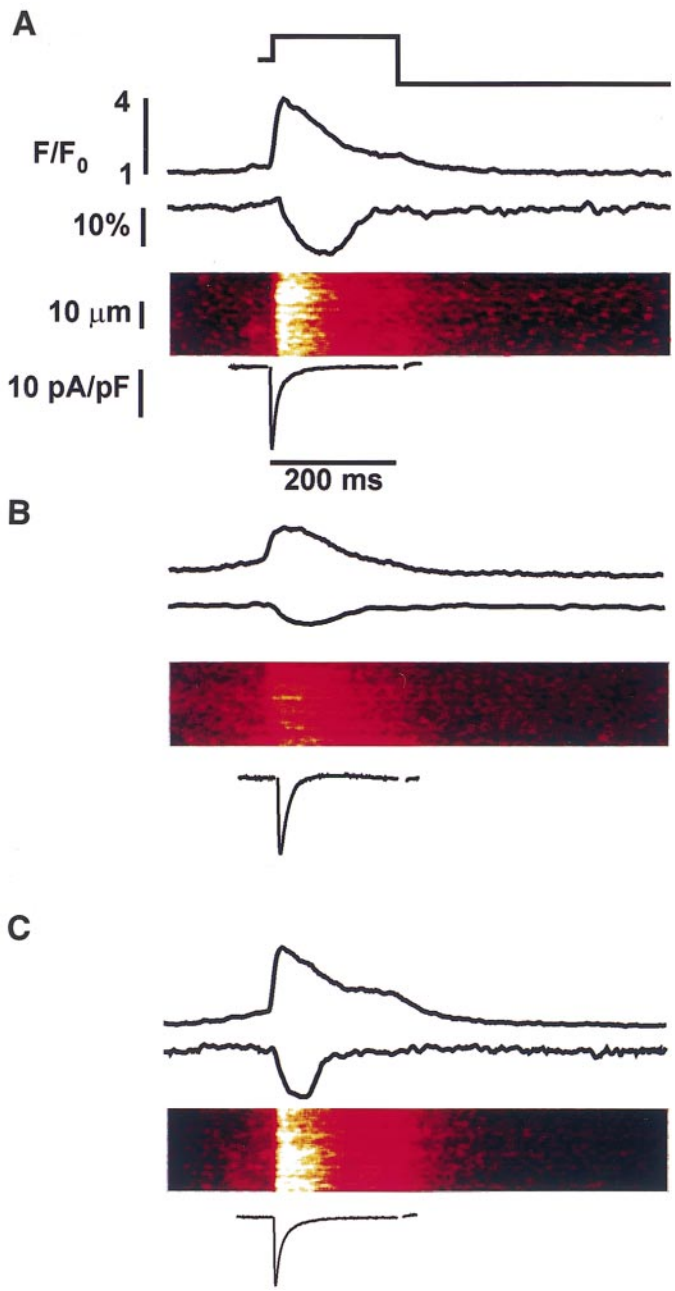

Fig. 5. Excitation-contraction coupling in mouse heart cells. Depolarization-activated intracellular Ca^{2+} concentration ($[Ca^{2+}]_i$) transients, membrane current, and contractions were examined in mouse myocytes using single-cell patch-clamp methods and confocal calcium imaging. Representative data from a wild-type ventricular myocyte (*A*), an MLP$^{-/-}$ myocyte (*B*), and a MLP$^{-/-}$/βARKct myocyte (*C*) are shown during a depolarization from −80 mV to 0 mV for 200 ms. The protocol involves first slowly (0.08 mV/ms) depolarizing the cell from −80 to −40 mV and holding the potential at −40 mV for 50 ms to inactivate Na^+ current and T-type Ca^{2+} current before depolarizing the cell to 0 mV for 200 ms. Top traces show a diagram of the voltage step from −40 mV to 0 mV and the repolarization step to −80 mV. The other components of each panel are (from *top* to *bottom*) the $[Ca^{2+}]_i$ transient (as fractional fluorescence, F/F_0), cell shortening (as % change from resting length), the line-scan image of $[Ca^{2+}]_i$, and the Ca^{2+} current (I_{Ca}) density (pA/pF). Line-scan images show time along the horizontal axis and position within the cell along the vertical axis. For all cells, sarcoplasmic reticulum (SR) Ca^{2+} content was controlled by a series of 4 conditioning depolarizations from −80 mV to 0 mV for 50 ms at 1 Hz (16, 37, 41) at 37°C. To measure SR Ca^{2+} load, caffeine (20 mM) was rapidly superfused over a test myocyte to evoke a $[Ca^{2+}]_i$ transient in a 0 mM Ca^{2+}, 0 mM Na^+ solution. The peak $[Ca^{2+}]_i$ level (F/F_0) was not significantly different in the 3 groups: wild type, 4.37 ± 0.39 ($n = 5$ cells); MLP$^{-/-}$, 4.11 ± 0.20 ($n = 6$ cells); MLP$^{-/-}$/βARKct, 4.74 ± 0.66 ($n = 5$ cells). Furthermore, lack of difference in the Ca^{2+} spark characteristics (size, shape, frequency) supports our conclusion that SR Ca^{2+} load was similar in the 3 groups.

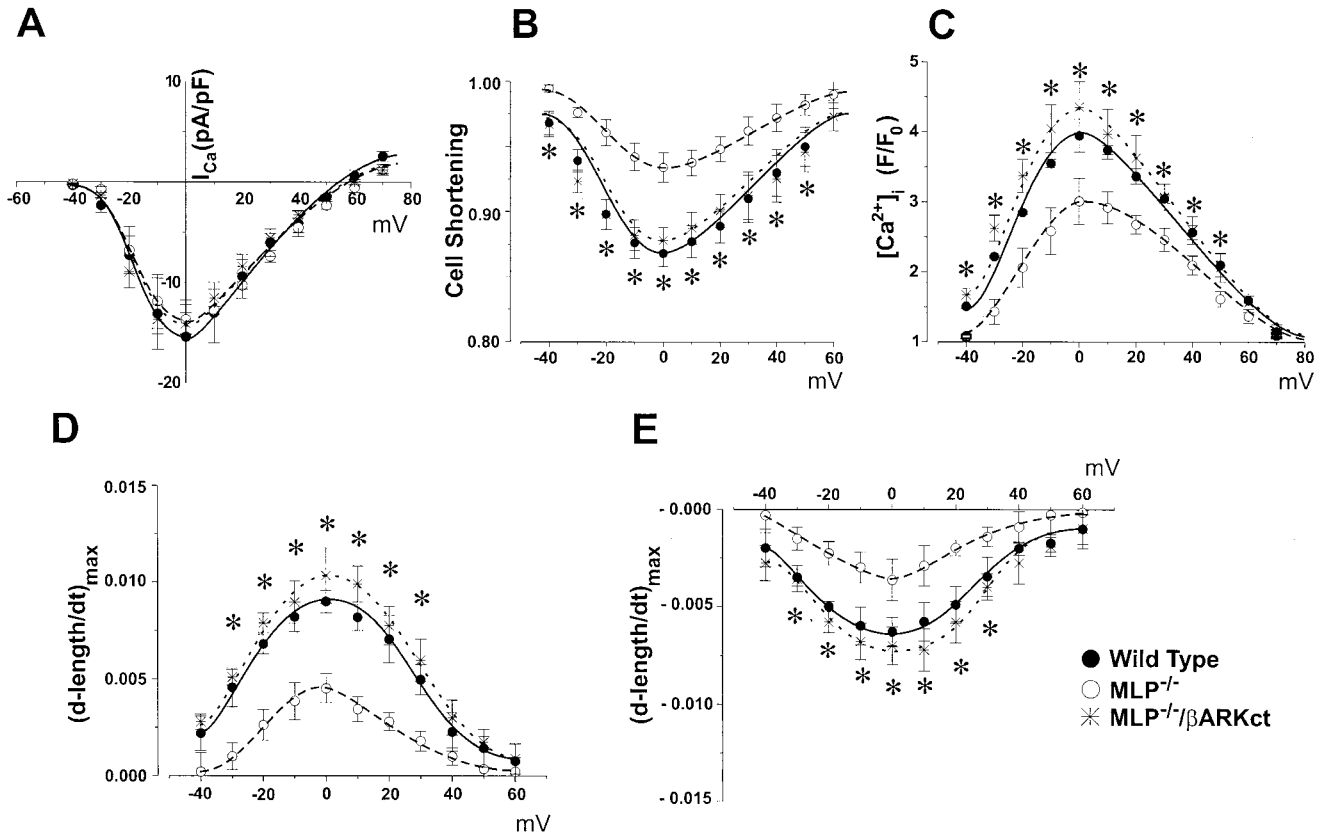

Fig. 6. Voltage-dependence of I_{Ca}, cell shortening, and the $[Ca^{2+}]_i$ transient. *A*: I_{Ca} plotted as current density (pA/pF) obtained for test potentials from −40 to +60 as shown in Fig. 5. Data from wild-type myocytes, MLP$^{-/-}$ myocytes, and MLP$^{-/-}$/βARKct myocytes are shown. *B*: cell shortening measurements as in *A*, plotted as fraction of resting length. *C*: $[Ca^{2+}]_i$ transient measurements (as F/F$_0$) as in *A*. *D*: rate of shortening during contraction of single cells as maximal first derivative of length [d(length)/dt_{max}]. *E*: rate of elongation during relaxation of single cells as d(length)/dt_{max}. *Significant differences ($P < 0.05$) in data from MLP$^{-/-}$ (n = 10 cells) and MLP$^{-/-}$/βARKct (n = 7 cells) compared with wild-type (n = 9) animals. Temperature = 37°C.

−20 mV [Fig. 7, *A* and *C*, *left*]. The plot of peak cell shortening vs. $[Ca^{2+}]_i$ shown in Fig. 8*A* for cells from the MLP$^{-/-}$/βARKct animals has returned toward control (see DISCUSSION). In our investigation of why the $[Ca^{2+}]_i$ transients returned to normal, we examined Ca^{2+} sparks and the EC coupling gain function in the cells from the MLP$^{-/-}$/βARKct animals. We found that the Ca^{2+} sparks in MLP$^{-/-}$/βARKct myocytes were similar to those in control cells. Because Ca^{2+} sparks in the MLP$^{-/-}$ myocytes were also identical to those in control cells, we learn about the functional similarity of the SR/T-tubular junction in the myocytes of the three types of mice we examined. We would conclude, therefore, that there is no significant difference in the ryanodine receptor cluster organization at SR/T-tubular junctions. Furthermore, because Ca^{2+} sparks in the MLP$^{-/-}$ myocytes were identical to those in the control myocytes, it also shows that there is no defect in SR Ca^{2+} uptake in the MLP$^{-/-}$ cells. However, as in other models of heart failure (8, 16, 34, 37, 41), there is a clear difference in the EC coupling gain function. In the experiments with MLP$^{-/-}$/βARKct mice, however, we find that the EC coupling gain function in cells from the MLP$^{-/-}$/βARKct animals has returned to normal.

DISCUSSION

To better understand the pathogenesis of heart failure and to explore novel treatments, we have examined the cellular and molecular defects that develop with well-defined models of heart failure (16, 41). Here we study a distinct model of heart failure that occurs when MLP is "knocked out" (i.e., the MLP$^{-/-}$ mouse) (1, 31). Echocardiographic abnormalities consistent with dilated cardiomyopathy and heart failure (1, 29, 31) are known, but intrinsic contractile and cellular defects have not been investigated until now (see Figs. 2–8). We have identified functional changes during in vivo measurements of cardiac pressure and volume consistent with an abnormality in intrinsic contractility. We have also observed an impaired β-AR response and a major defect in EC coupling that we identified as a decreased sensitivity of the SR Ca^{2+} release mechanism to triggering Ca^{2+}. There is an additional defect in Ca^{2+} signaling consistent with reduced sensitivity of the contractile proteins to Ca^{2+}. These findings in the MLP$^{-/-}$ animals are interesting because similar changes have been identified in other animal models of heart failure that are attributed to unrelated instigat-

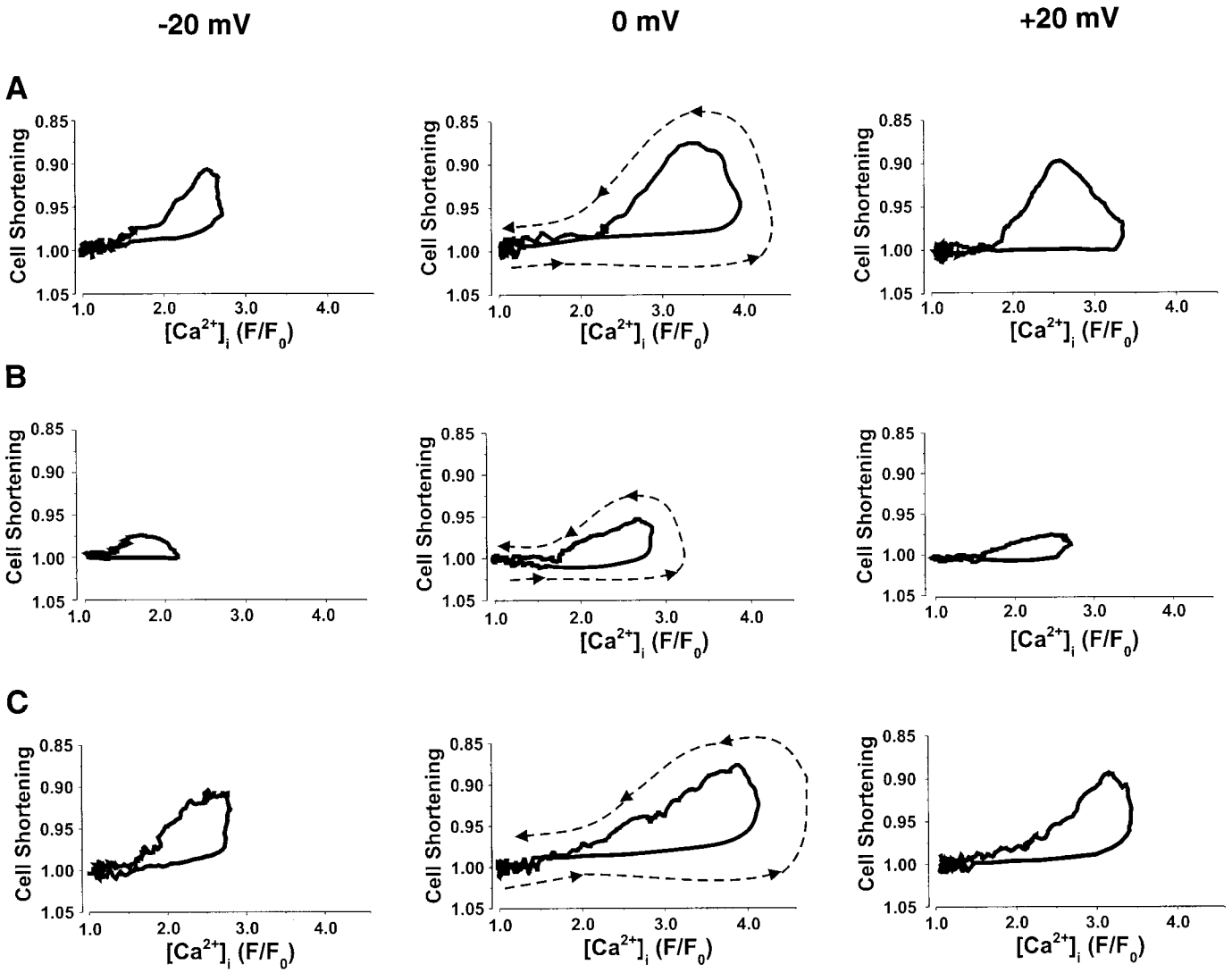

Fig. 7. Relationship between $[Ca^{2+}]_i$ and cell shortening during cellular contraction. The relationship between $[Ca^{2+}]_i$ and contraction (cell shortening) in heart cells during the contraction is plotted as a trajectory. Three depolarization potentials are shown −20 (*left*), 0 (*middle*), and +20 (*right*) mV. *A*: wild-type mice (n = 9 cells). *B*: $MLP^{-/-}$mice (n = 10 cells). *C*: $MLP^{-/-}$/βARKct mice (n = 7 cells). The voltage protocol is similar to that of Fig. 5. For each signal-averaged trace, the cells begin and end in a relaxed state at low $[Ca^{2+}]_i$. Thus the diagrams "begin" and "end" at the same point at the *bottom left corner*. The dashed lines with arrows indicate the counterclockwise trajectory of the relationship illustrated in Fig. 8*B*, *ii*, at 0 mV for *A*, *B*, and *C*. Temperature = 37°C.

ing insults [i.e., hypertension (16) or viral myocardiopathy (41)]. The most interesting and provocative finding, however, is that the heart failure pathology in $MLP^{-/-}$ animals can be almost completely recovered by the expression of a single transgene that functionally inhibits the action of βARK1. The most critical questions raised by these findings are discussed below.

Cellular and Molecular Mechanisms of Heart Failure

$MLP^{-/-}$ dilated cardiomyopathy. Because the MLPs are reported to link actin filaments together at the Z line, it has been argued that the absence of MLP may contribute to the development of dilated cardiomyopathy by the removal of its structural function (10) . The data presented here appear to argue against that simple conclusion. The reasoning is that there is virtually full recovery of cardiac contractile function in the $MLP^{-/-}$/βARKct animals and yet the MLP remains absent. Our conclusion is supported by Minamisawa et al. (29), who found that $MLP^{-/-}$ cardiomyopathy appears to be rescued by knocking out a different protein, phospholamban (PLB).

Initiating insult in $MLP^{-/-}$ animals. The data to date do not permit us to identify which feature of the $MLP^{-/-}$ pathology leads to the dilated cardiomyopathy, and thus allows the conclusion that some of the structural role of MLP is important. MLP, however, subserves many functions in addition to its putative structural role. MLP contributes to muscle development and serves as a nuclear transcription regulator

(10). There are no compelling data to date to indicate which of these many functions of MLP is critical to the development of dilated cardiomyopathy.

Why is the MLP$^{-/-}$ mouse rescued by cardiac-targeted expression of βARKct? We postulate that the MLP$^{-/-}$ dilated cardiomyopathy arises as the result of a pathological spiral that begins with the yet-unidentified initiating insult. The insult is inadequate to produce enormous contractile dysfunction on its own but can lead to sufficient dysfunction so that the β-AR system is activated in compensatory response. We reason that activation of the β-AR system is the primary means to increase cardiac output when it must be increased transiently. However, tonic activation of the β-ARs is not a normal response and becomes maladaptive because tonic β-AR occupancy by agonist increases β-AR desensitization and downregulation mediated in part by phosphorylation of receptors by βARK1. This hypothesis, first suggested by us (32), is supported by our findings presented here, where we show that there is virtually normal in vivo cardiac function with normalization of β-AR responsiveness in the MLP$^{-/-}$/βARKct mouse. This can be better understood in light of the restoration of cellular function in myocytes from these animals. Presumably, the main benefit of expressing the βARKct transgene in the hearts of the MLP$^{-/-}$ mice is the protection of β-ARs from chronic desensitization and downregulation.

We propose that normal β-AR function is important for the normal function of the heart. The β-AR, like other heptahelical receptors, not only serves to signal specific G protein-coupled effectors such as adenylyl cyclase but also signals a host of additional effectors through diverse intracellular proteins (17). Chronic downregulation and desensitization of β-ARs will blunt all cAMP-dependent protein kinase-mediated dependent signaling but will activate other intracellular pathways, such as those linked to cell growth (e.g., the mitogen-activated protein kinases) (25). We suggest that overexpression of the βARKct transgene reverses these maladaptations.

MLP$^{-/-}$/PLB$^{-/-}$ rescue of MLP$^{-/-}$. How effective is the MLP$^{-/-}$/PLB$^{-/-}$ rescue (see Ref. 29) compared with the MLP$^{-/-}$/βARKct rescue shown here? How does this rescue come about? Although we would like to know the answer to these questions, there is no way to address them properly at this time because neither P-V relations nor patch-clamp and confocal cellular $[Ca^{2+}]_i$

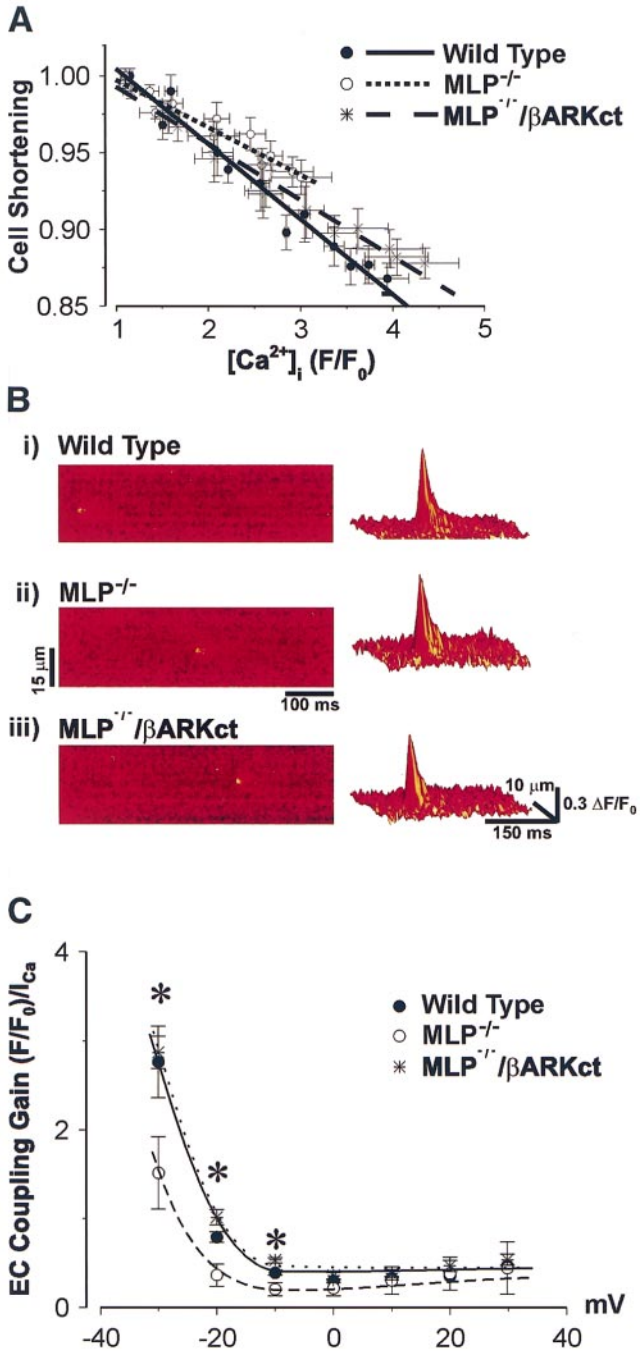

Fig. 8. Calcium signaling in heart cells. *A*: the relationship between cell shortening and $[Ca^{2+}]_i$ at peak $[Ca^{2+}]_i$ for ventricular myocytes taken from wild type (n = 9), MLP$^{-/-}$ (n = 10), and MLP$^{-/-}$/βARKct (n = 7) animals. These data points were chosen to reflect a "characteristic" of the relationships shown in Fig. 7 because the relationship rises vertically for a number of points at the maximal $[Ca^{2+}]_i$. Smooth lines represent linear fits to the data. Data were fit with a least-square routine using the equation: cell shortening = $a + b$ $[Ca^{2+}]_i$, where a and b used to fit the data were 1.054 ± 0.001 and −0.049 ± 0.001 (wild type), 1.028 ± 0.004 and −0.030 ± 0.003 (MLP$^{-/-}$), and 1.030 ± 0.004 and −0.037 ± 0.002 (MLP$^{-/-}$/βARKct), respectively. The correlation coefficients (R^2) for wild type, MLP$^{-/-}$, and MLP$^{-/-}$/βARKct were 0.99, 0.99 and 0.96, respectively. *B*: Ca^{2+} spark characteristics. Line-scan image (*left*) and signal-averaged surface plot of Ca^{2+} sparks (*right*) for typical Ca^{2+} spark in a wild-type heart cell (*i*), an MLP$^{-/-}$ heart cell (*ii*), and an MLP$^{-/-}$/βARKct heart cell (*iii*) are shown. Data were collected at a holding potential of −80 mV. Ca^{2+} spark frequency (sparks·100 μm^{-1}·s^{-1} ± SE) was found not to be significantly different: wild-type = 0.95 ± 0.18 (n = 10), MLP$^{-/-}$ = 0.75 ± 0.21 (n = 6), and MLP$^{-/-}$/βARKct = 1.07 ± 0.38 (n = 8). Ca^{2+} spark amplitude (F/F_0, ±SE) was also found not to be significantly different: wild-type = 1.63 ± 0.07 (n = 92), MLP$^{-/-}$ = 1.63 ± 0.05 (n = 109), and MLP$^{-/-}$/βARKct = 1.59 ± 0.05 (n = 27). *C*: EC coupling gain function $[(\Delta F/F_0)/I_{Ca}]$ is plotted as a function of voltage from multiple experiments in cells taken from wild-type (n = 9), MLP$^{-/-}$ (n = 10), and MLP$^{-/-}$/βARKct animals (n = 7). *P < 0.05, MLP$^{-/-}$ vs. either wild-type or MLP$^{-/-}$/βARKct. Temperature = 37°C. n, No. of cells studied in each group.

signals were studied in the $MLP^{-/-}/PLB^{-/-}$ mouse (29).

Fractional shortening in wild-type animals investigated by Minamisawa et al. (29) was quite low, as were heart rates, suggesting that the level of anesthesia may have been high and thus may have affected these measurements. We adjusted the level of anesthesia in our experiments to reduce potential toxicity and performed echocardiography under conscious conditions. Furthermore, heart rates measured during conscious echocardiography were similar to those obtained by telemetry in ambulatory mice, indicating little stimulation by the procedure (18). It is also interesting to note that the $MLP^{-/-}$ mice rescued by the PLB knockout did not regain β-AR responsiveness but remained in a highly stimulated state. This is similar to the result we found with cardiac-targeted expression of the β2-AR, which we showed to be deleterious in the $MLP^{-/-}$ mouse (31).

It is widely accepted that LV dP/dt_{max} provides useful information on relative changes in contractile behavior when all conditions are controlled in the same animal, (33); however, it has limited sensitivity when groups of different animals are compared (12, 27). In this regard, one of the best measures of cardiac contractile function in vivo is the P-V loop (23, 33), as we have used here.

P-V loops in the mouse. The analysis of P-V relations with the ESPVR has long been established as a standard method to evaluate cardiac function in larger species. This study in the mouse shows the nonlinear nature of the LV ESPVR (21, 30) and demonstrates how the shift of this relation can detect changes in contractility in the same heart but, most importantly, can identify differences in inotropic state between groups of genetically altered hearts. Recently, it was reported that ESPVRs were obtained by miniaturized conductance micromanometry (14). This study nicely demonstrates the utility of obtaining load-independent measures of ventricular performance to better understand the biology of disease using gene-targeted animals. Conversion to absolute volumes can be achieved using the hypertonic saline dilution method, but this can result in marked hemodynamic changes (42). In our study, we placed two orthogonal pairs of miniature piezoelectric crystals in the endocardial wall of the mouse heart. Because the output of the dimension crystal is a calibrated signal, we were able to obtain internal dimensions in two planes with high accuracy and therefore calculated absolute LV volume throughout the cardiac cycle. An important advantage of this technique is the ability to measure instantaneous wall thickness by placing an additional crystal on the epicardial surface juxtaposed to the endocardial crystal. This will allow for the calculation of wall stress throughout the cardiac cycle and will provide a method for the in-depth analysis of cardiac mechanics in gene-targeted murine hearts. It should be noted that the sonomicrometer technique requires open-chest instrumentation, which is technically demanding and will affect the measurement of basal hemodynamic parameters. For the assessment of murine cardiac function, this technique is complementary to that of closed-chest catheter-based hemodynamic and echocardiography measurements and provides an assessment of intrinsic in vivo contractile function in a load-independent manner.

In summary, a model of dilated cardiomyopathy with heart failure ($MLP^{-/-}$) was used to investigate cellular defects in heart failure and possible new therapies. We have extended our preliminary result (31) by examining the in vivo and cellular behavior of the relevant hearts. Importantly, we show that by expressing the cardiac-targeted βARKct transgene in $MLP^{-/-}$ animals a nearly complete restoration of contractile function can be achieved. The compelling restoration of function by transgenic expression of βARKct suggests that modeling the mechanism of action of the βARKct is an attractive therapeutic approach.

We gratefully acknowledge Debbie Colpitts for expert secretarial assistance.

This work was supported in part by National Heart, Lung, and Blood Institute Grants HL-61558 (H. A. Rockman) and HL-36974, HL-61602, and HL-25675 (W. J. Lederer). H. A. Rockman is a recipient of a Burroughs Wellcome Fund Clinical Scientist Award in Translational Research.

REFERENCES

1. **Arber S, Hunter JJ, Ross JJ, Hongo M, Sansig G, Borg J, Perriard JC, Chien KR, and Caroni P.** MLP-deficient mice exhibit a disruption of cardiac cytoarchitectural organization, dilated cardiomyopathy, and heart failure. *Cell* 88: 393–403, 1997.
2. **Bland JM and Altman DG.** Statistical methods for assessing agreement between two methods of clinical measurement. *Lancet* 1: 301–310, 1986.
3. **Bristow MR.** Changes in myocardial and vascular receptors in heart failure. *J Am Coll Cardiol* 22: 61A–71A, 1993.
4. **Bristow MR.** Mechanism of action of beta-blocking agents in heart failure. *Am J Cardiol* 80: 26L–40L, 1997.
5. **Bristow MR.** Why does the myocardium fail? Insights from basic science. *Lancet* 352, *Suppl* 1: SI8–SI14, 1998.
6. **Bristow M and Port JD.** Beta-adrenergic blockade in chronic heart failure. *Scand Cardiovasc J Suppl* 47: 45–55, 1998.
7. **Cannell MB, Cheng H, and Lederer WJ.** Spatial non-uniformities in $[Ca^{2+}]_i$ during excitation-contraction coupling in cardiac myocytes. *Biophys J* 67: 1942–1956, 1994.
8. **Cannell MB, Cheng H, and Lederer WJ.** The control of calcium release in heart muscle. *Science* 268: 1045–1050, 1995.
9. **Cheng H, Lederer WJ, and Cannell MB.** Calcium sparks: elementary events underlying excitation-contraction coupling in heart muscle. *Science* 262: 740–744, 1993.
10. **Chien KR.** Stress pathways and heart failure. *Cell* 98: 555–558, 1999.
11. **Cho MC, Rapacciuolo A, Koch WJ, Kobayashi Y, Jones LR, and Rockman HA.** Defective beta-adrenergic receptor signaling precedes the development of dilated cardiomyopathy in transgenic mice with calsequestrin overexpression. *J Biol Chem* 274: 22251–22256, 1999.
12. **Davidson DM, Covell JW, Malloch CI, and Ross J Jr.** Factors influencing indices of left ventricle contractility in the conscious dog. *Cardiovasc Res* 8: 299–312, 1974.
13. **Feldman AM.** Modulation of adrenergic receptors and G-transduction proteins in failing human ventricular myocardium. *Circulation* 87, *Suppl* 4: IV27–IV34, 1993.
14. **Georgakopoulos D, Christe ME, Giewat M, Seidman CM, Seidman JG, and Kass DA.** The pathogenesis of familial hypertrophic cardiomyopathy: early and evolving effects from an alpha-cardiac myosin heavy chain missense mutation. *Nat Med* 5: 327–330, 1999.

15. **Gómez AM, Cheng H, Lederer WJ, and Bers DM.** Ca^{2+} diffusion and sarcoplasmic reticulum transport both contribute to $[Ca^{2+}]_i$ decline during Ca^{2+} sparks in rat ventricular myocytes. *J Physiol (Lond)* 496: 575–581, 1996.
16. **Gómez AM, Valdivia HH, Cheng H, Lederer MR, Santana LF, Cannell MB, McCune SA, Altschuld RA, and Lederer WJ.** Defective excitation-contraction coupling in experimental cardiac hypertrophy and heart failure. *Science* 276: 800–806, 1997.
17. **Hall RA, Premont RT, and Lefkowitz RJ.** Heptahelical receptor signaling: beyond the G protein paradigm. *J Cell Biol* 145: 927–932, 1999.
18. **Jumrussirikul P, Dinerman J, Dawson TM, Dawson VL, Ekelund U, Georgakopoulos D, Schramm LP, Calkins H, Snyder SH, Hare JM, and Berger RD.** Interaction between neuronal nitric oxide synthase and inhibitory G protein activity in heart rate regulation in conscious mice. *J Clin Invest* 102: 1279–1285, 1998.
19. **Kass DA.** Clinical evaluation of left heart function by conductance catheter technique. *Eur Heart J* 13, *Suppl* E: 57–64, 1992.
20. **Kass DA.** Myocardial mechanics. In: *Heart Failure: Scientific Principles and Clinical Practice*, edited by Poole-Wilson P. New York: Churchill-Livingstone, 1997, p. 87–108.
21. **Kass DA, Beyar R, Lankford E, Heard M, Maughan WL, and Sagawa K.** Influence of contractile state on curvilinearity of in situ end-systolic pressure-volume relations. *Circulation* 79: 167–178, 1989.
22. **Kass DA, Grayson R, and Marino P.** Pressure-volume analysis as a method for quantifying simultaneous drug (amrinone) effects on arterial load and contractile state in vivo. *J Am Coll Cardiol* 16: 726–732, 1990.
23. **Kass DA and Maughan WL.** From "E_{max}" to pressure-volume relations: a broader view. *Circulation* 77: 1203–1212, 1988.
24. **Koch WJ, Rockman HA, Samama P, Hamilton RA, Bond RA, Milano CA, and Lefkowitz RJ.** Cardiac function in mice overexpressing the beta-adrenergic receptor kinase or a beta-ARK inhibitor. *Science* 268: 1350–1353, 1995.
25. **Lefkowitz RJ.** G protein-coupled receptors. III. New roles for receptor kinases and beta-arrestins in receptor signaling and desensitization. *J Biol Chem* 273: 18677–18680, 1998.
26. **Little WC and Braunwald E.** Assessment of cardiac function. In: *Heart Disease: A Textbook of Cardiovascular Medicine*, edited by Braunwald E. Philadelphia: Saunders, 1997, p. 421–444.
27. **Mahler F, Ross J Jr, O'Rourke RA, and Covell JW.** Effects of changes in preload, afterload and inotropic state on ejection and isovolumic phase measures of contractility in the conscious dog. *Am J Cardiol* 35: 626–634, 1975.
28. **Margossian SS, Anderson PA, Chantler PD, Deziel M, Umeda PK, Patel H, Stafford WF, Norton P, Malhotra A, Yang F, Caulfield JB, and Slayter HS.** Calcium regulation in the human myocardium affected by dilated cardiomyopathy: a structural basis for impaired Ca^{2+}-sensitivity. *Mol Cell Biochem* 194: 301–313, 1999.
29. **Minamisawa S, Hoshijima M, Chu G, Ward CA, Frank K, Gu Y, Martone ME, Wang Y, Ross J Jr, Kranias EG, Giles WR, and Chien KR.** Chronic phospholamban-sarcoplasmic reticulum calcium ATPase interaction is the critical calcium cycling defect in dilated cardiomyopathy. *Cell* 99: 313–322, 1999.
30. **Noda T, Cheng CP, De Tombe PP, and Little WC.** Curvilinearity of LV end-systolic pressure-volume and dP/dt_{max}-end-diastolic volume relations. *Am J Physiol Heart Circ Physiol* 265: H910–H917, 1993.
31. **Rockman HA, Chien KR, Choi DJ, Iaccarino G, Hunter JJ, Ross JJ, Lefkowitz RJ, and Koch WJ.** Expression of a beta-adrenergic receptor kinase 1 inhibitor prevents the development of myocardial failure in gene-targeted mice. *Proc Natl Acad Sci USA* 95: 7000–7005, 1998.
32. **Rockman HA, Koch WJ, and Lefkowitz RJ.** Cardiac function in genetically engineered mice with altered adrenergic receptor signaling. *Am J Physiol Heart Circ Physiol* 272: H1553–H1559, 1997.
33. **Sagawa K, Maughan WL, Suga H, and Sunagawa K.** *Cardiac Contraction and the Pressure-Volume Relationship*. New York: Oxford Univ. Press, 1988.
34. **Santana LF, Cheng H, Gómez AM, Cannell MB, and Lederer WJ.** Relation between the sarcolemmal Ca^{2+} current and Ca^{2+} sparks and local control theories for cardiac excitation-contraction coupling. *Circ Res* 78: 166–171, 1996.
35. **Santana LF, Gomez AM, Kranias EG, and Lederer WJ.** Amount of calcium in the sarcoplasmic reticulum—influence on excitation-contraction coupling in heart muscle. *Heart Vessels* 44–49, 1997.
36. **Santana LF, Gómez AM, and Lederer WJ.** Ca^{2+} flux through promiscuous cardiac Na^+ channels: slip-mode conductance. *Science* 279: 1027–1033, 1998.
37. **Santana LF, Kranias EG, and Lederer WJ.** Calcium sparks and excitation-contraction coupling in phospholamban-deficient mouse ventricular myocytes. *J Physiol (Lond)* 503: 21–29, 1997.
38. **Solaro RJ.** Is calcium the "cure" for dilated cardiomyopathy? *Nat Med* 5: 1353–1354, 1999.
39. **Solaro RJ and Rarick HM.** Troponin and tropomyosin: proteins that switch on and tune in the activity of cardiac myofilaments. *Circ Res* 83: 471–480, 1998.
40. **Ungerer M, Parruti G, Bohm M, Puzicha M, DeBlasi A, Erdmann E, and Lohse MJ.** Expression of beta-arrestins and beta-adrenergic receptor kinases in the failing human heart. *Circ Res* 74: 206–213, 1994.
41. **Wessely R, Klingel K, Santana LF, Dalton N, Hongo M, Lederer WJ, Kandolf R, and Knowlton KU.** Transgenic expression of replication-restricted enteroviral genomes in heart muscle induces defective excitation-contraction coupling and dilated cardiomyopathy. *J Clin Invest* 102: 1444–1453, 1998.
42. **Wu CC, Skaper SD, Schwenk TR, Mahler CM, Anne A, Finnerty PW, Haber HL, Weikle RM, and Feldman MD.** Accuracy of the conductance catheter for measurement of ventricular volumes seen clinically: effects of electric field homogeneity and parallel conductance. *IEEE Trans Biomed Eng* 44: 266–277, 1997.